



<b>Publication Year</b>	2015
<b>Acceptance in OA</b>	2020-03-30T15:02:11Z
<b>Title</b>	The Absolute Age of the Globular Cluster M15 Using Near-infrared Adaptive Optics Images from PISCES/LBT
<b>Authors</b>	Monelli, M., TESTA, Vincenzo, Bono, G., Ferraro, I., Iannicola, G., FIORENTINO, Giuliana, ARCIDIACONO, CARMELO, Massari, D., Boutsia, K., BRIGUGLIO PELLEGRINO, RUNA ANTONIO, BUSONI, LORENZO, CARINI, Roberta, Close, L., CRESCI, GIOVANNI, ESPOSITO, Simone, Fini, L., FUMANA, Marco, Guerra, J. C., Hill, J., Kulesa, C., MANNUCCI, FILIPPO, McCarthy, D., PINNA, Enrico, PUGLISI, Alfio Timothy, Quiros-Pacheco, F., RAGAZZONI, Roberto, RICCARDI, Armando, Skemer, A., XOMPERO, MARCO
<b>Publisher's version (DOI)</b>	10.1088/0004-637X/812/1/25
<b>Handle</b>	<a href="http://hdl.handle.net/20.500.12386/23708">http://hdl.handle.net/20.500.12386/23708</a>
<b>Journal</b>	THE ASTROPHYSICAL JOURNAL
<b>Volume</b>	812

## THE ABSOLUTE AGE OF THE GLOBULAR CLUSTER M15 USING NEAR-INFRARED ADAPTIVE OPTICS IMAGES FROM PISCES/LBT\*

M. MONELLI<sup>1,2</sup>, V. TESTA<sup>3</sup>, G. BONO<sup>3,4</sup>, I. FERRARO<sup>3</sup>, G. IANNICOLA<sup>3</sup>, G. FIORENTINO<sup>5</sup>, C. ARCIDIACONO<sup>5,6</sup>, D. MASSARI<sup>5,7</sup>,  
K. BOUTSIA<sup>3</sup>, R. BRIGUGLIO<sup>6</sup>, L. BUSONI<sup>6</sup>, R. CARINI<sup>3</sup>, L. CLOSE<sup>8</sup>, G. CRESCI<sup>5</sup>, S. ESPOSITO<sup>6</sup>, L. FINI<sup>6</sup>, M. FUMANA<sup>9</sup>,  
J. C. GUERRA<sup>10</sup>, J. HILL<sup>10</sup>, C. KULESA<sup>8</sup>, F. MANNUCCI<sup>6</sup>, D. MCCARTHY<sup>8</sup>, E. PINNA<sup>6</sup>, A. PUGLISI<sup>6</sup>, F. QUIROS-PACHECO<sup>6</sup>,  
R. RAGAZZONI<sup>11</sup>, A. RICCARDI<sup>6</sup>, A. SKEMER<sup>8</sup>, AND M. XOMPERO<sup>6</sup>

<sup>1</sup> Instituto de Astrofísica de Canarias, La Laguna, Tenerife, Spain; [monelli@iac.es](mailto:monelli@iac.es)

<sup>2</sup> Departamento de Astrofísica, Universidad de La Laguna, Tenerife, Spain

<sup>3</sup> INAF-Osservatorio Astronomico di Roma, Via Frascati 33, I-00040 Monteporzio Catone, Italy

<sup>4</sup> Università di Roma “Tor Vergata,” Via della Ricerca Scientifica 1, 00133 Roma, Italy

<sup>5</sup> INAF-Osservatorio Astronomico di Bologna, Via Ranzani 1, I-40127 Bologna, Italy

<sup>6</sup> INAF-Osservatorio Astronomico di Arcetri, Largo Enrico Fermi 5, I-50125 Firenze, Italy

<sup>7</sup> Kapteyn Astronomical Institute, Landleven 12, NL-9747 AD Groningen, The Netherlands

<sup>8</sup> Steward Observatory, Department of Astronomy, University of Arizona, Tucson, AZ 85721, USA

<sup>9</sup> INAF-IASF, via E. Bassini 15, I-20133 Milano, Italy

<sup>10</sup> LBT Observatory, University of Arizona, 933 North Cherry Ave., Tucson, AZ 85721, USA

<sup>11</sup> INAF-Osservatorio Astronomico di Padova, Vicolo dell’Osservatorio 5, I-35122, Padova, Italy

*Received 2014 November 6; accepted 2015 July 17; published 2015 October 6*

### ABSTRACT

We present deep near-infrared  $J$ ,  $K_s$  photometry of the old, metal-poor Galactic globular cluster M15 obtained with images collected with the LUCI1 and PISCES cameras available at the Large Binocular Telescope (LBT). We show how the use of First Light Adaptive Optics (FLAO) system coupled with the PISCES camera allows us to improve the limiting magnitude by  $\sim 2$  mag in  $K_s$ . By analyzing archival *Hubble Space Telescope* data, we demonstrate that the quality of the LBT/PISCES color–magnitude diagram is fully comparable with analogous space-based data. The smaller field of view is balanced by the shorter exposure time required to reach a similar photometric limit. We investigated the absolute age of M15 by means of two methods: (i) by determining the age from the position of the main-sequence turnoff (MSTO), and (ii) by the magnitude difference between the MSTO and the well-defined knee detected along the faint portion of the MS. We derive consistent values of the absolute age of M15, that is,  $12.9 \pm 2.6$  Gyr and  $13.3 \pm 1.1$  Gyr, respectively.

*Key words:* globular clusters: general – globular clusters: individual (M15) – techniques: photometric

### 1. INTRODUCTION

Cosmological results based on recent cosmic microwave background (CMB) experiments (Boomerang, *WMAP*, *Planck*), on baryonic acoustic oscillations (BAOs; Eisenstein et al. 2005), on supernova observations (Riess et al. 1998, 2011), and on gravitational lensing (Suyu et al. 2010, 2013) opened the path to the era of precision cosmology. However, the quoted experiments are affected by an intrinsic degeneracy in the estimate of cosmological parameters, e.g., the Hubble constant  $H_0$ . To overcome this problem, either specific priors or the results of different experiments are used (Bennett et al. 2014).

Recent evaluations of the  $H_0$  based on CMB provide values ranging from  $70.0 \pm 2.2$  km s<sup>−1</sup> Mpc<sup>−1</sup> (WMAP9; Hinshaw et al. 2013) to  $67.8 \pm 0.9$  km s<sup>−1</sup> Mpc<sup>−1</sup> (Planck Collaboration et al. 2015). Similar values have also been obtained by BAOs plus supernovae using the so-called inverse distance ladder, suggesting a value of  $68.6 \pm 2.2$  km s<sup>−1</sup> Mpc<sup>−1</sup> (Cuesta et al. 2015). On the other hand, resolved objects (Cepheids

plus supernovae) provide  $H_0$  values ranging from  $73 \pm 2$  (random)  $\pm 4$  (systematic) km s<sup>−1</sup> Mpc<sup>−1</sup> (Freedman & Madore 2010) to  $73.8 \pm 2.4$  km s<sup>−1</sup> Mpc<sup>−1</sup> (Riess et al. 2011). Slightly larger values of the Hubble constant were obtained by Suyu et al. (2013) using gravitational lens time delays ( $80.0^{+4.5}_{-4.7}$  km s<sup>−1</sup> Mpc<sup>−1</sup>, uniform  $H_0$  in flat  $\Lambda$ CDM).

The above estimates of the Hubble constant indicate that there is some tension between the results based on CMB and BAOs and those based on primary and secondary distance indicators. This critical issue has been addressed in several recent papers, suggesting a difference that ranges from almost  $2\sigma$  (Efstathiou 2014) to more than  $2.5\sigma$  (Riess et al. 2011). The quoted uncertainties on the Hubble constant open the path to new physics concerning the number of relativistic species and/or the mass of neutrinos (Dvorkin et al. 2014; Wyman et al. 2014). Moreover and even more importantly, the above range in  $H_0$  implies an uncertainty on the age of the universe— $t_0$ —of the order of 2 Gyr. This uncertainty has a substantial impact not only on galaxy formation and evolution but also on the age of the most ancient stellar systems, i.e., the globular clusters (GCs).

The absolute age of GCs can be independently estimated using stellar astrophysics, and it is affected by theoretical, empirical, and intrinsic uncertainties.

*Theoretical.*—Stellar evolutionary models adopted to construct cluster isochrones are affected by uncertainties in the

\* Observations were carried out using the Large Binocular Telescope at Mount Graham, AZ. The LBT is an international collaboration among institutions in the United States, Italy, and Germany. LBT Corporation partners are the University of Arizona on behalf of the Arizona university system; Istituto Nazionale di Astrofisica, Italy; LBT Beteiligungsgesellschaft, Germany, representing the Max-Planck Society, the Astrophysical Institute Potsdam, and Heidelberg University; the Ohio State University; and the Research Corporation, on behalf of the University of Notre Dame, University of Minnesota, and University of Virginia.

input physics, in particular, in the adopted microphysics (opacity, equation of state, astrophysical screening factors) and in macrophysics (mixing length, mass loss, atomic diffusion radiative levitation, color–temperature transformations). The impact that the quoted ingredients have on cluster isochrones has been discussed in detail in the literature (Pietrinferni et al. 2004, 2009; VandenBerg et al. 2013; Cassisi 2014). The typical uncertainty in the adopted clock—the main-sequence turnoff (MSTO)—is of the order of 10%, thus suggesting that theoretical uncertainties do not appear to be the dominant source in the error budget of the absolute age of GCs.

*Empirical.*—The main sources of uncertainty in the absolute age estimate of GCs are the individual distances ( $\Delta\mu_0 \sim 0.1$  mag in the true distance modulus implies an uncertainty of 1 Gyr in the absolute age). The age estimate is even more affected when the uncertainties in the reddening correction and in the reddening law are taken into account (Stetson et al. 2014).

Importantly, the massive use of multiobject fiber spectrographs provided the opportunity to construct a firm metallicity scale including a significant fraction of GCs (Carretta et al. 2009), thus reducing the uncertainties in the iron and in the  $\alpha$ -element abundances.

*Intrinsic.*—Dating back to more than 40 years ago, spectroscopic investigations brought forward a significant star-to-star variation in C and in N among cluster stars (Osborn 1971). This evidence was soundly complemented by variation in Na, Al, and O (Cohen 1978; Pilachowski et al. 1983; Leep et al. 1986) and by anticorrelations in CN–CH (Kraft 1994) and in O–Na and Mg–Al (Suntzeff & Smith 1991; Gratton et al. 2012).

The above evidence has been further strengthened by the occurrence of multiple stellar populations in more massive clusters (Bedin et al. 2004; Piotto et al. 2005, 2007). However, detailed investigations concerning the different stellar populations indicate a difference in age that is, in canonical GCs, on average shorter than 1 Gyr (Ventura et al. 2001; Cassisi et al. 2008). The intrinsic uncertainty does not seem to be the main source of the error budget of the GCs’ absolute age.

To overcome or to alleviate the quoted uncertainties, different approaches have been suggested, mainly based on relative age estimates, the so-called vertical and horizontal methods (Marín-Franch et al. 2009; Dotter et al. 2011; VandenBerg et al. 2013). In this context the relative age is estimated as a difference between the clock (the MSTO) and an evolved reference point, either the horizontal branch or a specific point along the red giant branch (RGB). The key advantage of these methods is that they are independent of uncertainties on cluster distance and reddening. However, they rely on the assumption that the reference points are independent of cluster age and introduce new theoretical uncertainties (conductive opacities, Cassisi et al. 2007; extra-deep mixing along the RGB, Denissenkov & Weiss 2004). It goes without saying that the transformation of relative ages in absolute ages using a calibrating GC introduces the typical uncertainties already discussed.

More recently it has been suggested to use as a reference point a well-defined knee along the low-mass regime of the main sequence (MSK). The MSK has already been detected in several old ( $\omega$  Cen, Pulone et al. 1998; M4, Pulone et al. 1999; Milone et al. 2014; Braga et al. 2015; NGC 3201, Bono et al. 2010; 47 Tuc, Lagioia et al. 2014; NGC 2808, Milone

**Table 1**  
Basic Parameters adopted for M15

Parameter	Value	References
$(m - M)_0$ (mag)	15.14	Harris (1996), Durrell & Harris (1993)
$E(B - V)$ (mag)	0.08	Sandage et al. (1981)
[Fe/H]	−2.4	Kraft & Ivans (2003)

et al. 2012; M71, Di Cecco et al. 2015) and intermediate-age (An et al. 2009a, 2009b; Sarajedini et al. 2009b) stellar systems and in the Galactic bulge (Zoccali et al. 2000) by using near-infrared (NIR) and/or optical–NIR color–magnitude diagrams (CMDs).

Nevertheless, one of the most difficult observational problems in measuring stellar magnitudes and colors in GCs is that they are intrinsically crowded stellar systems, and therefore the photometry of their stars is strongly limited by poor weather conditions. In particular, bad seeing (larger than  $\sim 1''$ ) has the effect of severely limiting the identification and measurement of faint stars. This means a systematic increase in the limiting magnitudes and in the photometric accuracy when moving from the outskirts to the innermost cluster center.

Twenty-five years ago the advent of the *Hubble Space Telescope* (HST) started a new era, and the high spatial resolution provided by space images collected in optical bands allowed us to resolve the core of GCs. Recently, a similar resolution is becoming possible from ground-based observations using NIR cameras available on 10 m class telescopes assisted by adaptive optics (AO) systems. This technology allows ground-based observations to reach the diffraction limit over a modest field of view (FOV;  $\sim 1' \times 1'$ ). High-resolution NIR images of GCs can have a relevant impact on current astrophysical problems as soundly demonstrated by MAD (Multi-Conjugated Adaptive Optics Demonstrator; Marchetti et al. 2003), the pilot Very Large Telescope (VLT) instrument built to test on the sky the feasibility of a multi-conjugate AO (MCAO) system (Bono et al. 2009; Ferraro et al. 2009; Moretti et al. 2009; Fiorentino et al. 2011). The robustness of the current MCAO systems has been further supported by GeMS/GSAOI available at the GEMINI-South telescope (Neichel et al. 2014a, 2014b; Rigaut et al. 2014). This new system uses both natural guide stars for the tip tilt correction and five artificial stars to close the loop, and it has been able to deliver uniform NIR images approaching its diffraction limit in Galactic bulge (Saracino et al. 2015) and halo (Turri et al. 2015) GCs.

In this context we have collected AO images of the GC M15 (NGC 7078), using the First Light Adaptive Optics (FLAO; Esposito et al. 2010) system mounted on the Large Binocular Telescope (LBT). This cluster is located at  $\approx 10$  kpc (10.4 kpc, Durrell & Harris 1993; 9.9 kpc, McNamara et al. 2004; 10.4 kpc, van den Bosch et al. 2006) and is affected by moderate interstellar extinction ( $E(B - V) = 0.08$  mag, Sandage et al. 1981; 0.10, Schlafly & Finkbeiner 2011, 0.12, Schlegel et al. 1998). Most interestingly, it is among the most metal-poor Galactic GCs ([Fe/H]  $\approx -2.4$ ; Kraft & Ivans 2003), and therefore it possibly traces the oldest component of our Galaxy (see Table 1 for the parameters assumed in our analysis). Notably, despite multiple populations having been proved to exist in this cluster (Monelli et al. 2013; Piotto et al. 2015), so far there is no evidence of multiple turnoff or subgiant branches

**Table 2**  
Observation Log

Telescope	Sensor	Filter	Exposures (s)	Total Time (s)
LBT	LUCI1	$J$	$13 \times 20 \ 13 \times 40$	780
		$K_s$	$26 \times 40$	1040
	PISCES	$J$	$20 \times 30$	600
		$K_s$	$42 \times 15$	630
HST	WFC3	$F160W$	$3 \times 200 \ 6 \times 250$	2100

as for NGC 1851 (Milone et al. 2008) that could affect the age estimate.

## 2. OPTICAL AND NIR DATA SETS

The present work uses four different data sets from different imagers. In the following we summarize the main properties of each of them. A summary is given in Table 2.

### 2.1. LBT/PISCES Data

PISCES is an NIR imager covering a wavelength range of 1–2.5  $\mu\text{m}$  with a Hawaii 1024 pixel  $\times$  1024 pixel HgCdTe array, installed at the front bent-Gregorian focus (McCarthy et al. 2001) of the LBT. It critically samples a diffraction-limited point-spread function (PSF) with a plate scale of  $0''.0193 \text{ pixel}^{-1}$ . Observations were carried out using PISCES, together with the FLAO system mounted on the DX (right) telescope of LBT. M15 was observed on 2011 October 14–15 during the Science Verification Time for the FLAO system. This is a twin of the 672-actuator, voice-coil-based, contactless adaptive mirror (Salinari et al. 1994; Davies et al. 2010) controlled by the means of a pyramid (Ragazzoni 1996) wavefront sensor. The FLAO uses solely the Natural Guide Star as reference, and it retrieves a high Strehl ratio over a broad wavelength range, reaching peak performance on a bright reference in the NIR (80% in the  $H$  band). Once at the regime phase, the two FLAO systems will feed the LUCI1 and LUCI2 cameras (Le Fèvre et al. 2003).

Two fields were acquired with the FLAO+PISCES setup, one centered on the cluster core, the other approximately  $3'$  southwest of the cluster center. In both cases the selection criterion for the field was the presence of a suitable star for wavefront analysis in the FOV, with magnitude  $R = 12.6 \text{ mag}$  and  $R = 12.9 \text{ mag}$  for the central and outer field, respectively. In the current investigation we will focus on the external field. A preliminary photometric analysis of the central field, together with a detailed investigation of the variation of the PSF across the FOV, has already been discussed by Fiorentino et al. (2014). A comprehensive analysis will be addressed in a forthcoming investigation. During the observations, weather conditions were photometric with good natural seeing conditions ( $0''.65$ – $0''.9$ , as recorded by the DIMM). The AO allowed us to reach a mean FWHM of  $0''.05$  and of  $0''.06$  in the  $J$  and in the  $K_s$  band, respectively, as measured on the images. The Strehl ratio on the quoted images reached 28% ( $J$ ) and 60% ( $K_s$ ) consistently with the expected scaling versus wavelength.

### 2.2. LBT/LUCI1 Data

One pointing with the spectro-imager LUCI1 at LBT was collected for calibration purposes. The set of observations was secured on 2012 June 21–22 in the  $J$  and  $K_s$  filters, under good

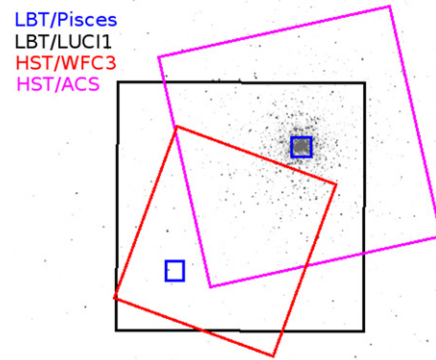


**Figure 1.** SDSS image of M15 superimposed with the fields of the different data sets collected for this project. Detailed analysis of the central PISCES field will be presented in a forthcoming paper.

seeing conditions ( $\sim 0''.7$ ). The data set was taken with the center of the cluster in the NE quadrant of the image in order to include both the central and the outer field observed with PISCES. We adopted this observing strategy to constrain possible systematics in the absolute calibrations due to positional effects. An off-source set of images was also taken to perform median-sky subtraction and superflat construction (see Section 2.4).

### 2.3. HST Optical and NIR Data

Complementary data sets will be used in the analysis of the LBT images. In particular, a series of nine images has been retrieved from the HST archive. They were collected with the WFC3 in the  $F160W$  passband. Furthermore, we will make use of  $F606W$  and  $F814W$  photometry of M15, retrieved from the “Advanced Camera for Surveys (ACS) Survey of Galactic GCs” database (Sarajedini et al. 2007).

Figure 1 shows a Sloan Digital Sky Survey (SDSS) image of M15 superimposed with the footprint of the adopted cameras: LUCI1 (black square), PISCES (blue), ACS (magenta), and WFC3 (red). The LUCI1 field ( $4' \times 4'$ ) was selected so as to include both the center of the cluster and the PISCES field, which is located  $2'.7$  from the center. Note the small FOV covered by the PISCES camera ( $21'' \times 21''$ ). The HST/ACS field is centered on M15, but owing to the different position angle, it does not overlap with the PISCES pointing, which on the other hand falls into the HST/WFC3 set. Figure 2 presents a comparison of the LBT/LUCI1 (left), HST/WFC3 (center), and LBT/PISCES (right) regions, corresponding to the full FOV of the PISCES camera. Other than the impressive improvement when comparing data from the same telescope but without (left panel) and with (right panel) assistance from the AO, it is clear that PISCES provides the best spatial resolution also when compared to the WFC3 (middle panel). It is worth noting that the three images are stacked medians; thus, the total exposure time is different in the three cases. Moreover, while the left and right panels show images in the  $K_s$ , we only had available WFC3 images in the  $F160W$  filter, which is close to the  $H$  band. To highlight even more the PISCES performances, Figure 3 shows a zoom-in of the PISCES (left) and WFC3 (right) stacked images already shown in Figure 2. The green squares mark a region of  $5'' \times 5''$ . The image discloses at first glance that the number of sources is similar in both cases, suggesting a similar limiting magnitude (it is worth

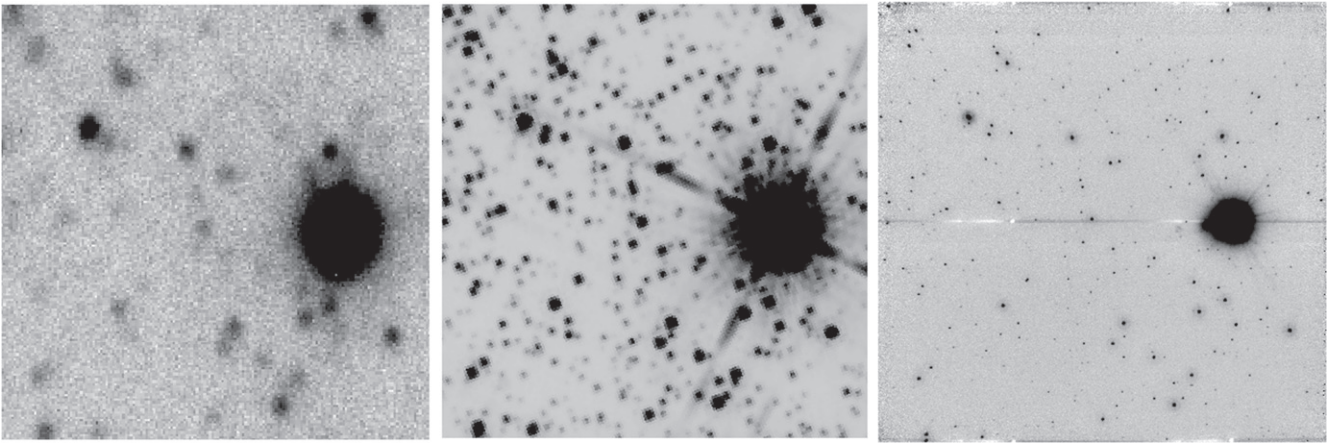


**Figure 2.** Sky region covered by the PISCES camera (right) as seen also by LUCI1 (left) and the WFC3 (middle). Note the change in spatial resolution, from  $0''.118 \text{ pixel}^{-1}$  (seeing limited),  $0''.13 \text{ pixel}^{-1}$  (from space),  $0''.026 \text{ pixel}^{-1}$ .

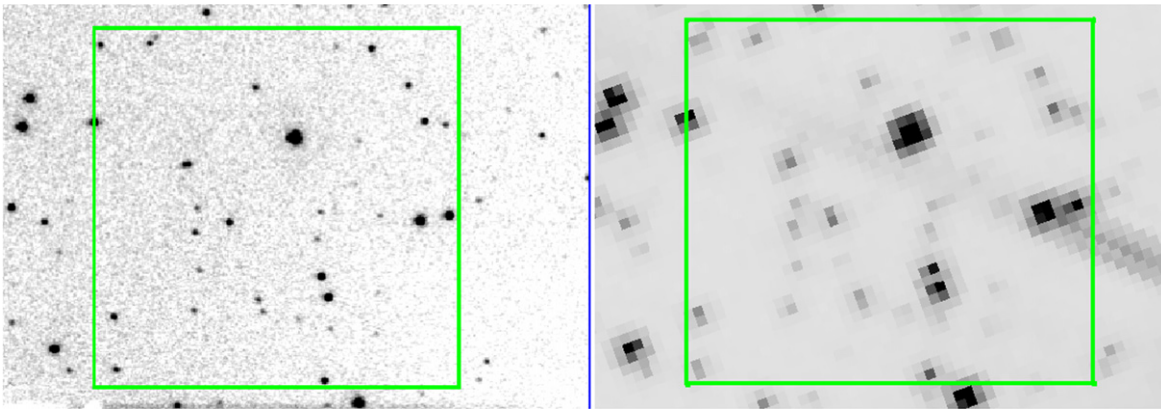


**Figure 3.** Zoom-in on the same PISCES (left) and WFC3 (right) images of Figure 2. The green square highlights the same sky region of  $5'' \times 5''$ . The comparison clearly shows the gain in spatial resolution of the PISCES data.

recalling here the shorter total exposure time in both PISCES  $J$  and  $K_s$ ; see Table 2). On the other hand, the contrast in the PISCES images is by far better, and one can easily see that elongated sources in the WFC3 field are well separated in the PISCES image, such as those next to the top left corner of the green square.

#### 2.4. Data Reduction and Photometry

The acquisition and the basic reduction have been performed following a homogeneous approach for both PISCES and LUCI1 data: raw images have been secured by dithering the telescope within a 100 pixel random pattern to ensure good removal of bad pixels. Single images have been dark-subtracted, flat-fielded, resampled to remove geometrical distortions, and registered. For the  $K_s$  filter, a superflat obtained with the off-source sky images has been obtained and applied to the images to improve the low-frequency flat-field removal.

The LUCI1 and WFC3 data have been independently reduced following the prescriptions of Monelli et al. (2010) and using a standard procedure based on the DAOPHOTIV/ALLSTAR/ALLFRAME suite of programs (Stetson 1987, 1994). Individual PSFs have been modeled for each image, using semiautomatic routines. The input list of stars for ALLFRAME was generated registering and matching the individual catalogs from single images.

The case of the PISCES data deserved particular attention, because AO may provide PSFs characterized by spatial variations across the field due to anisoplanatism. This is especially true for the shorter-wavelength  $J$ -band images, while the PSF in the  $K_s$  is typically more stable even at the largest distances from the guide stars, as it scales with the isoplanatic angle and progressively with the wavelength. Therefore, to perform the photometry on these images, we adopted the ROMAFOT suite of programs (Buonanno et al. 1983; Buonanno & Iannicola 1989). The PSF photometry with ROMAFOT is more lengthy when compared with similar packages available in the literature. However, it has the key advantage of a graphical interface that allows the user to improve the local deconvolution of stellar profiles. The latest version of the code (I. Ferraro et al. 2015, in preparation) has been optimized to perform accurate photometry of crowded stellar fields on images collected with AO systems. In particular, it takes into account the spatial variation of the PSF across the FOV and the variation of the asymmetric, egg-like shape of the PSF. A preliminary discussion of the numerical algorithms and of the approach adopted to deal with the quoted images has already been presented in Fiorentino et al. (2014). In passing, we note that photometry performed using asymmetric PSFs on ground-based (LBT/LUCI1) and space (*HST*/WFC3) images gives magnitudes that are, within the errors, identical to those measured using other photometric packages.

The final adopted photometry was obtained in two steps. First, ROMAFOT was run on the mean  $J$ - and  $K_s$ -band images in order to create the master list of objects. The final photometry was obtained reducing the individual images and averaging the derived magnitudes. A Moffat analytic function was adopted to model the PSF, with  $\beta = 2.0, 2.5$  and  $\sigma = 2.70, 2.05$  for the  $J$  and  $K_s$  images, respectively.

The final photometric catalogs were calibrated into the Two Micron All Sky Survey (2MASS) photometric system in two steps. First, the LUCI1 photometric catalog was calibrated using  $\sim 200$  stars in common with 2MASS and covering the entire FOV. Then three dozen local standards of the LUCI1 catalog were used to calibrate the photometric catalog based on PISCES images. In this context it is worth mentioning the crucial role that faint local standards play in the accurate calibration of images collected with AO systems. The use of NGS for the tip-tilt correction and the modest FOV of current AO systems imply the selection of crowded stellar fields. In these cluster regions the photometric quality of the 2MASS local standards is quite poor; moreover, even the faintest 2MASS stars are saturated in these regions. These are the reasons why the calibration of NIR images collected with AO systems does require a double step in the calibration using 4–8 m class telescopes to improve the limiting magnitude and the photometric accuracy of local standards (Bono et al. 2010).

Keeping in mind the above caveats, Figure 4 shows the approach we adopted to perform the absolute calibration. From left to right, the three rows show the residuals of the calibration as a function of magnitude (top:  $J$ ; bottom:  $K_s$ ), the  $X$  coordinate, and the  $Y$  coordinate. Small dots indicate the 2MASS stars in common with LUCI1, while the open squares show the  $\sim 35$  LUCI1 stars used as a local standard to calibrate the PISCES catalog. No apparent trends are visible, and the residuals have null mean.

### 3. RESULTS

Figure 5 shows NIR CMDs of the central regions of M15 based on four different imagers. From left to right, the ( $K_s, J - K_s$ ) CMD is based on (a) LBT/LUCI1 covering an FOV of 16 arcmin squared ( $\sim 17,000$  stars); (b) the intersection of space  $F160W$ -band (*HST*/WFC3) and ground-based  $K_s$ -band (LBT/PISCES) photometry covering an FOV of 0.19 arcmin squared ( $\sim 380$  stars); and (c) LBT/PISCES covering an FOV of 0.19 arcmin squared ( $\sim 450$  stars). The jump in limiting magnitude is compelling when moving from seeing-limited (LBT/LUCI1, (b)) to AO (LBT/PISCES, (c)) NIR images collected with the same telescope. Indeed, the use of the PISCES camera, together with the FLAO (Esposito et al. 2012; Riccardi et al. 2010), allows us to move the limiting magnitude in the  $K$  band down to  $\approx 22.5$ – $23.0$  mag. To our knowledge this is the deepest  $K_s$ -band photometry ever performed in a GC.

Panel (d) shows a direct comparison between the CMD of the stars in common with PISCES (large black dots) and LUCI1 (green plus signs). The two overlap over a magnitude range of  $\approx 3.5$  mag, from  $K_s \approx 16.6$  mag to  $K_s \approx 20.1$  mag. The main sequence based on PISCES images is narrower than the LUCI1 one, and no systematics appear in the comparison (see also Figure 4). Interestingly enough, the sequence of green symbols plotted in panel (a) discloses a smaller photometric dispersion than the bulk of the main-sequence stars in the LUCI1 field. The difference is mainly due to the low crowding level of these cluster regions. Indeed, the 450 stars measured in

the PISCES FOV imply a density of  $0.67$  stars arcsec $^{-2}$ , that is, one star every  $\sim 2330$  pixel $^2$ . This context is quite different when compared with the central pointing, since in this region the typical stellar density is a factor of  $\approx 50$  higher.

The CMD based on LUCI1 images allows the identification of the typical evolutionary features of a GC. It covers more than 10 mag in the  $K_s$  band and ranges from the tip of the RGB ( $K_s \sim 9.5$  mag) down to  $\sim 2$  mag below the MSTO ( $K_s \sim 18, J - K_s \sim 0.25$  mag). Moreover, M15 also shows a well-populated horizontal branch ranging from  $K_s \sim 16.5$  to  $K_s \sim 14$  mag with a slope typical of NIR CMDs. Finally, the RGB bump appears clearly in the luminosity function of the RGB at magnitude  $K_s = 13.00 \pm 0.05$  mag, indicated by the arrow.

In spite of the good quality of LUCI1 photometry, it is thanks to PISCES and to the FLAO system that we have been able to identify, for the first time, the MSK ( $K_s \sim 21.5$  mag) in a very metal-poor GC. The quality of the CMD based on LBT/PISCES is further supported by the comparison with the CMD based on both space- and ground-based NIR images. Data plotted in panel (d) of Figure 5 show that the limiting magnitude in  $F160W$  is similar to the limiting magnitude in the  $J$  band. However, the intrinsic error at fixed magnitude seems larger in  $F160W$  than in the  $J$ -band CMD, and indeed the MSK cannot be easily identified in the above CMD. In passing, we also note that the exposure time in  $F160W$  is 3.5 times larger than the exposure time in the  $J$  band.

We are dealing with photometric catalogs that have been collected using different telescopes equipped with different imagers and different sets of filters. Their possible systematics might affect the absolute age estimates. To constrain this effect, Figures 6 and 7 show the comparison of selected cluster isochrones with our data. A glance at the data plotted in this figure clearly shows the advantage of using CMDs based on optical and NIR photometric data. Indeed, the optical–NIR CMDs do cover a range in color that is at least a factor of two larger compared with the optical ones. From left to right, Figure 6 shows (a) the optical CMD based on ACS images ( $F606W, F606W - F814W$ ); (b) the optical–NIR CMD based on ACS and on WFC3 images ( $F606W, F606W - F160W$ ); (c) the optical–NIR CMD based on ACS and on LUCI1  $J$ -band images ( $F606W, F606W - J$ ); and (d) the optical–NIR CMD based on ACS and on LUCI1  $K$ -band images ( $F606W, F606W - K_s$ ). The cluster isochrone was computed by adopting the evolutionary tracks provided by VandenBerg et al. (2014). The isochrones were transformed into the observational plane by adopting the color–temperature relation by Casagrande & VandenBerg (2014). We adopted an iron abundance of  $[\text{Fe}/\text{H}] = -2.4$  (Kraft & Ivans 2003), an  $\alpha$ -enhancement of  $\alpha = +0.4$  (Snedden et al. 1997, 2000), primordial helium content of  $Y = 0.25$ , and a cluster age of 13 Gyr (red line). The current theoretical framework is fully consistent with the set of isochrones adopted by Bono et al. (2010). We performed a series of tests to constrain the optimal true distance modulus and reddening that provide a good simultaneous agreement between theory and observations in the four CMDs plotted in Figure 5. We found, using the Cardelli et al. (1989) reddening law, that a cluster reddening of  $E(B - V) = 0.08$  mag and a distance modulus of  $(m - M)_0 = 15.14$  mag (Harris 1996, 2010 edition) do provide a good agreement in the quoted optical–NIR CMDs. The cluster reddening agrees with the value suggested by Sandage et al. (1981) but is marginally

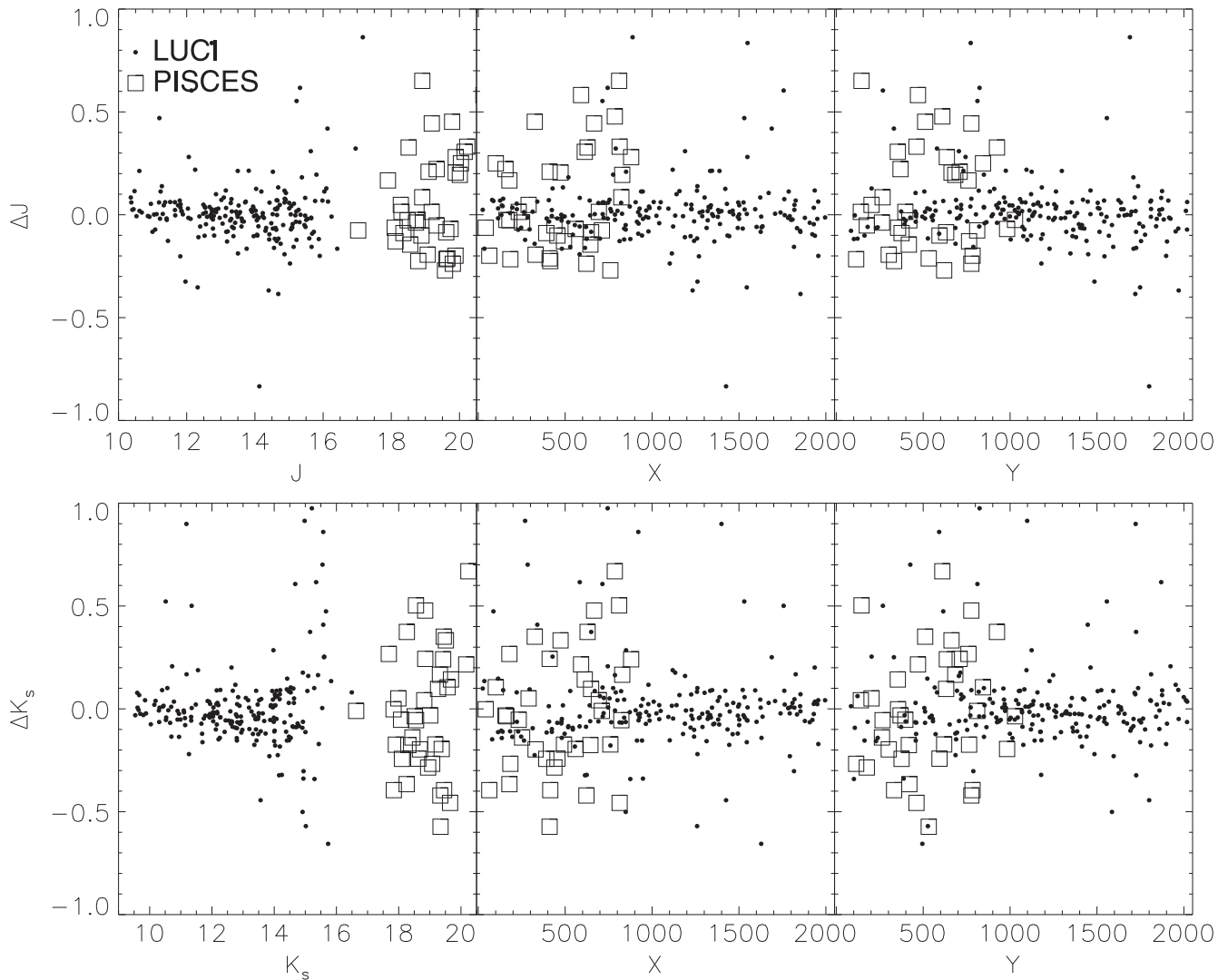


**Figure 4.** Residuals of the calibrations as a function of magnitude (left),  $X$  coordinate (middle), and  $Y$  coordinate (right). Top and bottom rows refer to the  $J$  and  $K_s$  bands, respectively. Large dots show the more than 200 stars in common between the LUCI catalog and 2MASS. Big open squares compare the  $\sim 35$  stars in common between LUCI and PISCES, at significantly fainter magnitude. Note that the ranges of  $X$  and  $Y$  are different because of the size of the two cameras.

smaller than the more recent estimates by Schlafly & Finkbeiner (2011) ( $E(B - V) = 0.10$ ). The true distance modulus agrees, within the errors, with different estimates available in the literature (Durrell & Harris 1993; van den Bosch et al. 2006). Note that the assumption of a larger extinction would imply, at fixed age, a systematic drift of the isochrones toward redder colors. The new discrepancy could be alleviated by a decrease in cluster age, but younger isochrones are characterized by a slope of the subgiant branch (SGB) that is too steep when compared with the data. This difference becomes more evident in the optical planes, where the SGB is remarkably thin. The above evidence indicates that adopted distance and reddening are mainly constrained by the morphology of the SGB and RGB, the former one playing a crucial role, since it is less affected by uncertainties in the adopted mixing length (Salaris & Cassisi 2015).

The CMDs plotted in panels (c) and (d) also suggest a good agreement between theory and observations. Indeed, only a marginal shift in color is present at the base of the RGB in the  $F606W$ ,  $F606W - J$  CMD. The anonymous referee also noted a similar shift in the RGB region between the HB and the

base of the RGB. In the quoted cases, the isochrones are once again marginally redder than the observed RG stars. The above empirical evidence brings forward two relevant points:

1. Theory and observations disclose an overall very good agreement over more than 10 mag. The agreement becomes even more compelling if we take account of the fact that we are dealing with optical and NIR data collected with space- and ground-based facilities. This finding also supports the adopted chemical composition, the bolometric corrections, and the color-temperature transformations, together with the adopted true distance modulus and cluster reddening. Similar results have also been obtained in the literature by different groups (Dotter et al. 2008; Sarajedini et al. 2009a; Bressan et al. 2012; Dell’Omodarme et al. 2012; VandenBerg et al. 2014), thus further supporting the current accuracy era of stellar astrophysics.

2. The difference in color at the level of 0.03 mag between theory and observations has a marginal impact on the methods we are using to estimate the absolute cluster age. Indeed, they rely either on absolute (MSTO) or on relative magnitudes (MSK).

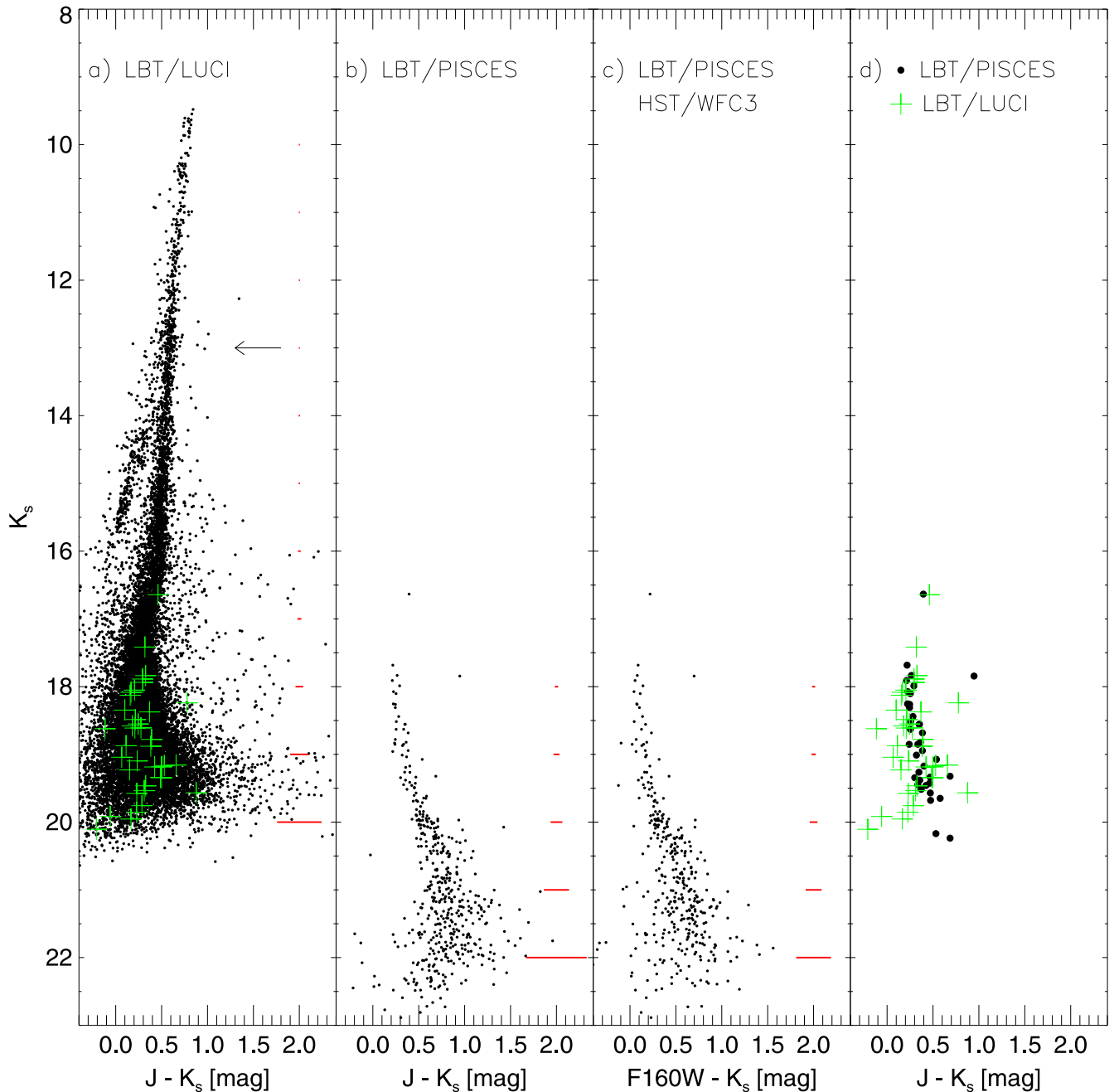


**Figure 5.** ( $K_s$ ,  $J - K_s$ ) CMDs of M15. (a) Data from LBT/LUCI1. The horizontal arrow marks the position of the RGB bump. The green plus signs show the stars in common with the PISCES photometry. (b) LBT/PISCES CMD of the outer M15 field. (c) Mixed CMD with *HST*/WFC3 [*F160W*] together with LBT/LUCI1 [ $K_s$ ] data. (d) Comparison of the CMD of the stars in common between LUCI1 (green plus signs as in panel (a)) and PISCES (large black dots).

Figure 7 shows a comparison with isochrones for different assumptions on the  $\alpha$  enhancement and the metal content. The left panel presents two isochrones of 12 (red line) and 13.5 Gyr (green). The effect of age appears clearly in the MSTO region, but as expected, it affects neither the RGB nor the low main sequence. The right panel present two isochrones of 13 Gyr, with  $[\text{Fe}/\text{H}] = -2.2$  and  $-2.4$  (red and green line, respectively) for different age and metallicity assumptions.

#### 4. THE ABSOLUTE AGE OF M15

To estimate the absolute age of M15, we devise here a double approach. The first is based on the MSTO position, and the second on the magnitude difference between the MSTO and

the main MSK. Table 3 summarizes the observables and the cluster ages based on the two quoted methods. From left to right the columns give the adopted CMD, the imager, the apparent magnitude, the color index of the MSTO ( $m_{\text{MSTO}}$ ,  $\text{CI}_{\text{MSTO}}$ ), and the color index of the MSK ( $m_{\text{MSK}}$ ,  $\text{CI}_{\text{MSK}}$ ), together with the two cluster ages.

##### 4.1. The TO Method

The position of the MSTO is determined in the observational planes to be the bluest MS point of the ridge line. Similarly, we estimate the magnitude and color index of the MSTO for a set of four isochrones of fixed metallicity ( $[\text{Fe}/\text{H}] = -2.4$ ,  $\alpha = +0.4$ ,  $Y = 0.25$ ) and age between 12.0 and 13.5 Gyr (see

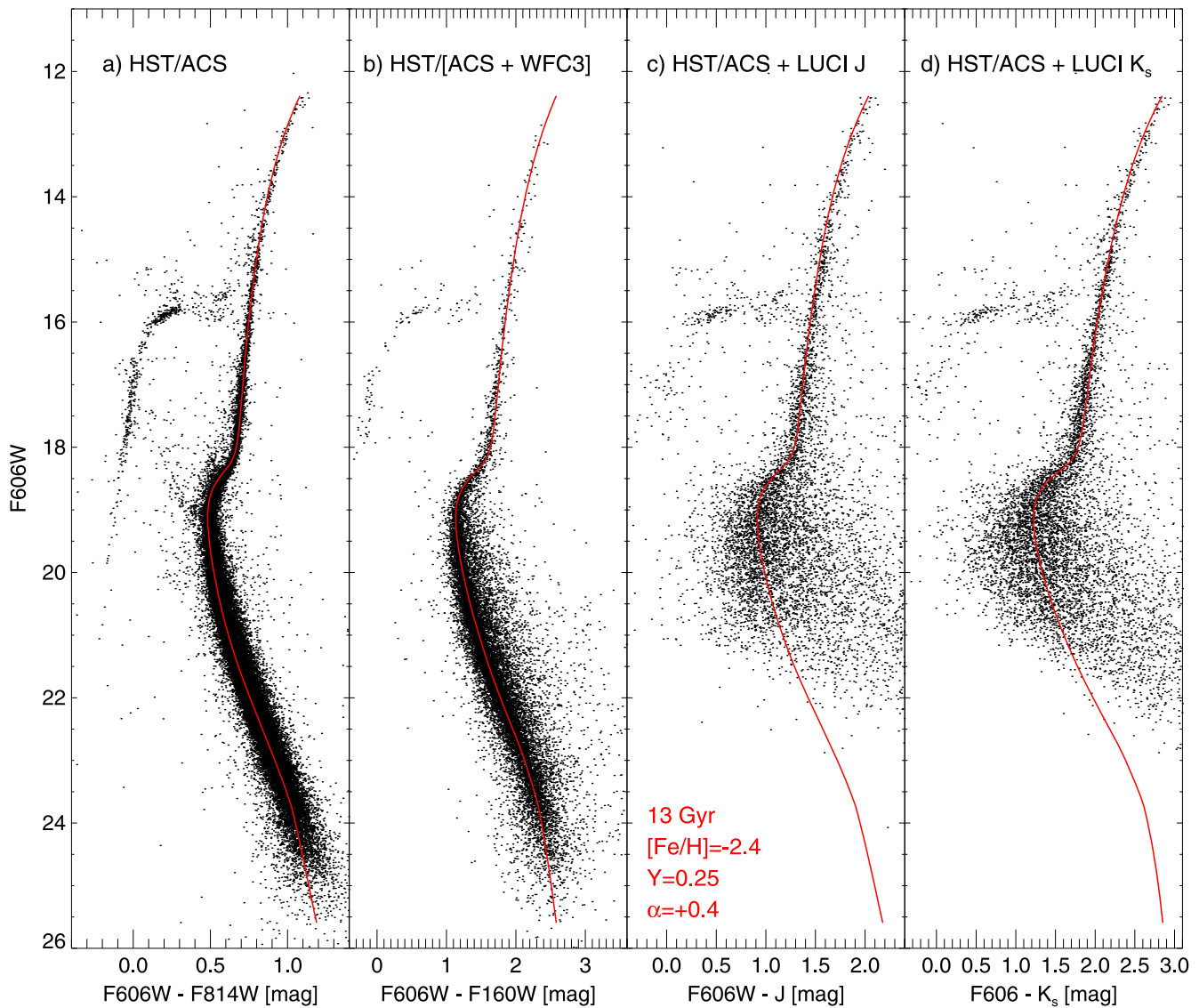


Figure 6. Optical and NIR CMDs based on *HST* data superimposed with the same isochrone for the labeled parameters.

Section 3) once rescaled for the proper distance and reddening. This allows us to determine that, at least in this age range, a linear relation exists between the MSTO magnitude and the age. The slopes of the above relations were obtained with a linear least-squares fit. The coefficients are listed in Table 4, together with the predicted magnitudes of the MSTO and of the MSK as a function of cluster age. These slopes are a measure of the sensitivity of the MSTO as an age indicator in the different bands. For example, we derive that the  $F606W$  band is  $\sim 1.8$  times more accurate than the  $K_s$  band.

The age corresponding to M15 is derived by interpolating the previous relations assuming the observed MSTO magnitude. The error budget has to take into account various sources, including error on the photometric calibration, the MSTO magnitude, the reddening, and distance.<sup>12</sup> In the case of the present data set, the photometric error varies depending on the filter used, from  $\sim 0.011$  in the case of the  $F814W$  filter to

$\sim 0.04$  mag for the LUCI1  $K_s$ . Nevertheless, while the differential reddening is almost negligible along the line of sight of M15 ( $E(B - V) = 0.08 \pm 0.01$  mag; Sandage et al. 1981), the dominant source of error is the distance ( $\pm 0.15$  mag; Durrell & Harris 1993). We derive an absolute age ranging from  $12.8 \pm 2.0$  ( $F814W$  band) to  $14.0 \pm 3.0$  Gyr ( $K_s$ ), with a weighted mean value of  $12.9 \pm 2.6$  Gyr.

#### 4.2. The MSK Method

The second approach is based on the magnitude difference between the MSTO and the MSK,  $\Delta M$  (MSTO - MSK). This method is based on the fact that the magnitude and color of the MSK in the low-mass regime of the MS are, at fixed chemical composition, essentially independent of cluster age (Bono et al. 2010). The key advantage of the MSK is that it is caused by collision-induced absorption opacities of both  $H_2-H_2$  and  $H_2-He$  in the surface of cool dwarfs (Borysow et al. 2001; Borysow 2002). The MSK is independent of cluster age and anchored in a region of the MS that is marginally affected by uncertainties in the treatment of the convective regime that is nearly adiabatic (Saumon & Marley 2008). Recent empirical

<sup>12</sup> The error in the age is totally dominated by the propagated error in the distance estimate. We note that the distance value from van den Bosch et al. (2006) provides an error a factor of 2 smaller, which would imply a reduction of  $\sim 30\%$  on the error on the absolute age determined with the MSTO.

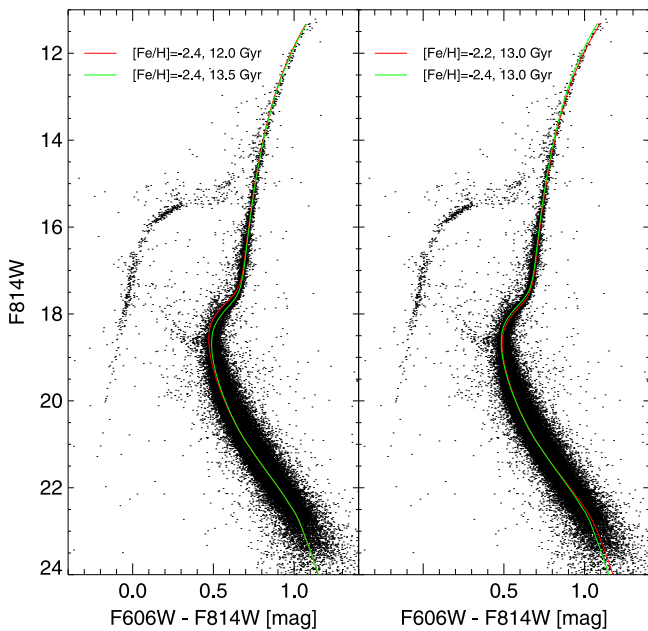


**Figure 7.** Comparison with isochrones of different ages (left) and metallicities (right).

evidence indicates that the errors in the absolute age of GCs based on this method are on average a factor of two smaller than the canonical ones (Bono et al. 2010; Di Cecco et al. 2015).

Therefore, this method offers a powerful observable to constrain the cluster age either as a color or as a magnitude difference between the bend and the cluster MSTO, using both optical and infrared filter combinations. In the case of the present data set, we determined the position of both points using the ridge line of the cluster in the different CMDs (see, e.g., Di Cecco et al. 2015). Note that the lack of a sizable sample of MSTO stars in the PISCES photometry is a direct consequence of the modest FOV covered by the camera and by the radial distance of the pointing. To constrain on a more quantitative basis this relevant issue, we selected the same cluster region covered by PISCES in the LUCI1 photometry, and we found that it only includes 35 stars and that the bulk of them are located at magnitudes fainter than the MSTO (see panel (d) of Figure 5).

To overcome this issue, we merged the LUCI1 and PISCES CMDs and derived a unique ridge line. In this way, the TO region is sampled by the large number of stars in the LUCI1 photometry, while the MSK is sampled by the PISCES deep catalog. In particular, following Bono et al. (2010), we define the color and magnitude of the MSK at the maximum curvature point in the low part of the MS. The outcome is shown in Figure 8, where the combined LUCI1 and PISCES CMDs are shown, together with the cluster ridge line, the MSTO, and the MSK. The approach adopted to compute the cluster ridge line has been discussed in detail by Di Cecco et al. (2015). The corresponding theoretical points were estimated using the same approach on the same isochrones adopted to estimate the cluster absolute age with the canonical MSTO method.

Similarly to the age determination based on the MSTO, we derive linear relations between  $\Delta M(\text{MSTO} - \text{MSK})$  and the age (see Table 4). In this case, the method is slightly more sensitive than adopting the absolute value of the MSTO, by

$\sim 15\%$ . The age is therefore derived by interpolating the empirical value derived from the CMDs, and it is reported in the last columns of Table 3. The estimated age ranges from  $12.9 \pm 0.9$  ( $F606W$  band) to  $13.7 \pm 1.0$  Gyr ( $K_s$ ), with a mean value of  $13.3 \pm 1.1$  Gyr.

#### 4.3. Comparison with Literature Values

The values shown in the last two columns of Table 3 disclose a general good agreement between the two derived age values. The estimate derived with the ( $K_s, J - K_s$ ) CMD is marginally higher than the other ones, but still well within the error bars. Also, the age derived with the MSTO is 0.3–0.9 Gyr smaller than the corresponding value derived with the MSK approach.

The age of M15 has been subject to a large number of investigations (e.g., Salaris et al. 1997; Salaris & Weiss 1998, 2002; McNamara et al. 2004; De Angeli et al. 2005). We stress that a straight comparison of literature estimates is complicated by the different theoretical scenarios adopted. However, the age derived here is in good agreement with recent estimates available in the literature ( $12.8 \pm 0.6$  Gyr, Marín-Franch et al. 2009;  $12.75 \pm 0.25 \pm 1.5$  Gyr, VandenBerg et al. 2013). Notably, these estimates are based on a difference approach. The former analysis uses the relative age of a population of clusters, anchored to an absolute scale using clusters with well-determined distance (NGC 6752 via the subdwarf-based method). The latter uses the absolute magnitude of the MSTO. Note that we are using the same set of optical data as VandenBerg et al. (2013), and indeed we independently obtain a perfectly consistent value of the age based on the MSTO luminosity, close to 12.8 Gyr.

## 5. DISCUSSION

### 5.1. Comparison with NGC 3201 and Metallicity Dependence

In the present work we studied NIR photometry of the very metal-poor cluster M15. Nonetheless, it is interesting to extend the analysis to a more metal-rich regime in order to explore the dependency of the  $\Delta M(\text{MSTO} - \text{MSK})$  method on both the age and the metallicity of the target system. Bono et al. (2010) presented a similar analysis for the cluster NGC 3201 ( $[\text{Fe}/\text{H}] \sim -1.5$ ). By adopting the same theoretical framework applied here, we derive analogous linear relations correlating the magnitude difference  $\Delta M(\text{MSTO} - \text{MSK})$  with age, assuming  $[\text{Fe}/\text{H}] = -1.5$ . The obtained derivatives (e.g.,  $0.13 \pm 0.01 \text{ mag Gyr}^{-1}$  and  $0.08 \pm 0.01 \text{ mag Gyr}^{-1}$  for the  $F606W$  and the  $K_s$  band, respectively) are very similar to those derived for more metal-poor isochrones suitable for M15. This supports that the  $\Delta M(\text{MSTO} - \text{MSK})$  diagnostic can be fruitfully used over a wide range of metallicities.

Moreover, by comparing the absolute position of the MSK in different isochrones, we find that (i) at fixed metallicity, the magnitude of the MSK changes by at most 0.02 mag, for ages larger than 10.5 Gyr; (ii) similarly, at fixed age the MSK moves by  $\sim 0.02$  mag, when moving from  $[\text{Fe}/\text{H}] = -2.4$  to  $[\text{Fe}/\text{H}] = -1.5$ . Interestingly, these values seem independent of the wavelength, at least in the spectral range covered by the  $F606W$  to  $K_s$  the passbands. Overall, the position of the MSK seems to be a reliable anchor, marginally dependent on the age and the metallicity, at least in the ranges investigated so far. However, a more systematic theoretical investigation is needed, in order to constrain in detail the sensitivity of the MSK, and in

**Table 3**  
Age Determinations

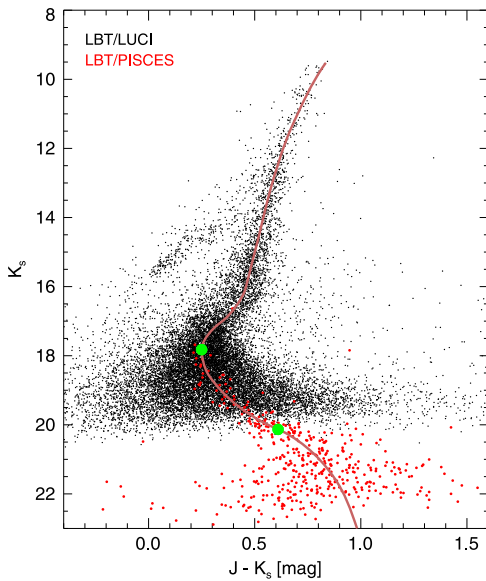
CMD	Cameras	$m_{\text{MSTO}}$	$\text{CI}_{\text{MSTO}}$	$m_{\text{MSK}}$	$\text{CI}_{\text{MSK}}$	$t_{\text{MSTO}}$	$t_{\text{MSTO-MSK}}$
$F814W, F606W - F814W$	ACS	$18.801 \pm 0.011$	$0.490 \pm 0.016$	$21.642 \pm 0.036$	$0.829 \pm 0.052$	$12.8 \pm 2.0$	$13.3 \pm 0.6$
$F160W, F814W - F160W$	WFC3+ACS	$18.027 \pm 0.040$	$0.652 \pm 0.041$	$20.296 \pm 0.051$	$1.045 \pm 0.059$	$12.5 \pm 2.7$	$13.4 \pm 1.3$
$F160W, F606W - F160W$	WFC3+ACS	$18.027 \pm 0.040$	$1.147 \pm 0.041$	$20.377 \pm 0.051$	$1.838 \pm 0.061$	$12.6 \pm 2.7$	$12.9 \pm 1.3$
$K_s, J - K_s$	PISCES	$18.010 \pm 0.043$	$0.238 \pm 0.044$	$20.160 \pm 0.290$	$0.581 \pm 0.299$	$14.0 \pm 3.1$	$13.7 \pm 1.4$

**Table 4**  
Magnitude vs. Age Derivatives

Mag	$d\text{Mag}(\text{TO})/dt$	$d\text{Mag}(\text{TO-MSK})/dt$
$F606W$	$0.09 \pm 0.01$	$0.11 \pm 0.01$
$F814W$	$0.08 \pm 0.01$	$0.09 \pm 0.01$
$J$	$0.06 \pm 0.02$	$0.07 \pm 0.02$
$F160W$	$0.06 \pm 0.01$	$0.07 \pm 0.01$
$K_s$	$0.05 \pm 0.02$	$0.06 \pm 0.02$

Mag	$d\text{CI}(\text{TO})/dt$	$d\text{CI}(\text{TO-MSK})/dt$
$F606W - F814W$	$0.01 \pm 0.01$	$0.02 \pm 0.01$
$F606W - F160W$	$0.03 \pm 0.01$	$0.02 \pm 0.01$
$J - K_s$	$0.01 \pm 0.01$	$0.01 \pm 0.01$

**Figure 8.** ( $K, J - K$ ) CMDs from LBT data (black: LUCI1; red: PISCES) superimposed with the derived ridge line. The big dots mark the MSTO and MSK points.

turn of the  $\Delta M$  (MSTO – MSK) method, over the full range of ages and metallicities typical of Galactic GCs.

### 5.2. Cosmological Implications

There is mounting evidence that we are in the era of precision cosmology. Recent estimates of the Hubble constant suggest a precision of the order of 3% ( $74.3 \pm 2.1 \text{ km s}^{-1} \text{ Mpc}^{-1}$ , Freedman et al. 2012;  $73.8 \pm 2.4 \text{ km s}^{-1} \text{ Mpc}^{-1}$ , Riess et al. 2011). Plain physical arguments suggest that, in a flat universe, the age of the universe ( $t_0$ ) is connected with the Hubble constant ( $H_0$ ), the matter density parameter ( $\Omega_m$ ), and the dark energy density

( $\Omega_\Lambda$ ) by the following relation (Dekel et al. 1997):

$$t_0 = [1 - (\Omega_m - 0.7\Omega_\Lambda)/5.8]/(1.3 \times h_0) \quad (1)$$

where  $h_0 = H_0/100 \text{ km s}^{-1} \text{ Mpc}^{-1}$  is the current expansion rate of the universe and  $t_0$  is the age of the universe today in units of  $10^{10}$  Gyr.

Using the recent estimates of the cosmological parameters provided by *WMAP* and *Planck* ( $\Omega_m = 0.315^{+0.016}_{-0.018}$ ,  $\Omega_\Lambda = 0.685^{+0.018}_{-0.016}$ ; Hinshaw et al. 2013; Planck Collaboration et al. 2014), we found  $t_0 = 10.70 \pm 0.82$  Gyr.<sup>13</sup> The above cosmological age is within  $1\sigma$  of current stellar ages. However, it is on the short limit if we also take account of the time for structure formation ( $z \sim 8$ ,  $t < 1$  Gyr). A similar approach to constrain the age of the universe today is to use, together with the above cosmological parameters, the estimate of  $H_0$  provided by *Planck+WMAP* ( $H_0 = 67.3 \pm 1.2 \text{ km s}^{-1} \text{ Mpc}^{-1}$ ). It is worth mentioning that  $H_0$  is a prior in the CMB solution ranging from 20 to  $100 \text{ km s}^{-1} \text{ Mpc}^{-1}$ . Note that in this context the precision on  $H_0$  is of the order of 1.8%. The age of the universe we found is  $t_0 = 11.75 \pm 0.21$  Gyr, while the detailed inversion of the CMB maps provides  $t_0 = 13.817 \pm 0.048$  Gyr. The above estimates appear in quite good agreement with the current absolute ages of oldest GCs, and we note that a smaller age of  $10.71 \pm 0.50$  Gyr is derived assuming the  $H_0$  value from Riess et al. (2011).

However, we are facing the evidence that the uncertainties on cosmological ages are systematically smaller than 1 Gyr for estimates based on  $H_0$  and become smaller than a few hundreds of Myr for CMB determinations. On the other hand, the uncertainties affecting the absolute age of GCs range from 2 (MSTO) to 1 (MSK) Gyr. The difference in precision between cosmological and stellar ages is going to become even more prominent, since the next generation of experiments (Riess et al. 2011; Freedman et al. 2012) plans to improve by a factor of two the precision on  $H_0$ . Taken at face value, the “stellar” estimates do not allow us to validate the evaluations provided by cosmology. It is clear that accurate absolute ages for a sizable sample of extremely metal-poor GCs can shed new light on this long-standing and intriguing problem.

## 6. CONCLUSIONS AND FUTURE REMARKS

We have presented new NIR data of the metal-poor GC M15 obtained with the LUCI1 and PISCES cameras available at the LBT, and complemented with archival optical and NIR *HST* data. The analysis of the data raised important points: (i) the ground-based AO camera can compete with the *HST* in terms of photometric depth and resolving power in moderately crowded stellar fields, with a smaller investment of telescope

<sup>13</sup> Note that we did not assume an Einstein–de Sitter cosmological model ( $\Omega_m = 1, \Omega_\Lambda = 0$ ) because the age of the universe we obtain is systematically younger ( $t_0 = 8.6 \pm 0.28$  Gyr) than suggested by recent “stellar” and “cosmological” estimates.

time; (ii) tests performed with the ROMAFOT package suggest that the data reduction of images from the AO instrument requires the development of novel techniques to model the complicated PSF of these imagers.

The MSK is an important feature in the CMD of GCs that can help revise the age of these fundamental stellar systems. The obvious advantage of using the  $\Delta M$  (MSTO – MSK) approach, being a differential measurement, is that it is not affected by the errors either in the distance or in the reddening. This is reflected in the significantly smaller error bars in the age determinations. The analysis presented in this paper reveals that different photometric bands provide different sensitivity to the method. In this sense, the sensitivity decreases for increasing wavelength from the optical to the near-infrared.

Our data analysis allowed us, using the PISCES data, to measure the MSK along the main sequence of M15. We use two diagnostics to estimate the absolute age of this cluster: the magnitude of the MSTO and the magnitude difference  $\Delta M$  (MSTO – MSK). The two methods provide consistent results and a mean absolute age of  $12.9 \pm 2.6$  Gyr and  $13.0 \pm 1.1$  Gyr, respectively.

A systematic theoretical analysis of the dependence of the MSK magnitude over a wide range of ages and metallicities is mandatory to firmly establish the uncertainties affecting the  $\Delta M$  (MSTO – MSK) method. Nonetheless, our results suggest that using high-quality, optical databases such as those based on existing *HST* data can provide a fundamental starting point to globally revise the age of the GC systems. The PISCES data presented here soundly demonstrate the potential of ground-based NIR data using AO technology to obtain deep photometry in crowded stellar fields. Moreover, current ongoing observing facilities at the 10 m class telescopes using either SCAO (FLAO at LBT) or MCAO (GEMS at Gemini South) are providing excellent data reaching the MSK in many Galactic GCs (NGC 1815, Turri et al. 2014, 2015). The same outcome applies to near-future facilities such as ERIS at ESO VLT. Nevertheless, a giant leap forward is foreseeable when the next generation of extremely large telescopes, equipped with NIR detectors and AO systems (e.g., Deep et al. 2011; Greggio et al. 2012; Schreiber et al. 2014), is available: the Giant Magellan Telescope (GMT),<sup>14</sup> the Thirty Meter Telescope (TMT),<sup>15</sup> and the European Extremely Large Telescope (E-ELT).<sup>16</sup>

Realistic predictions according to up-to-date instrumental specifications for the E-ELT+Maory+Micado configuration suggest that the predicted limiting magnitude ( $K \sim 27.2$  assuming a crowding level expected for the core of a GC; e.g., Deep et al. 2011), is significantly fainter than the expected MSK magnitude for any stellar system in the Milky Way halo (within 100 kpc, MSK  $\sim 24.5$ ). This is true also when restricting to a relatively short integration time of 600 s, comparable with that of the PISCES data presented in this paper. Preliminary analysis suggests that the error bar on the age will be smaller than 1 Gyr for the entire sample of GCs. This means that we will be able to successfully apply this method, for the first time, also to the nearby Local Group galaxies and their GCs.

The authors warmly thank Don VandenBerg for sharing the new set of isochrones prior to publication. Support for this work has been provided by the Education and Science Ministry of Spain (grant AYA2010-16717). G.F. has been supported by the Futuro in Ricerca 2013 (grant RBFR13J716). This work was partially supported by PRIN–INAF 2011 “Tracing the formation and evolution of the Galactic halo with VST” (P.I.: M. Marconi) and by PRIN–MIUR (2010LY5N2T) “Chemical and dynamical evolution of the Milky Way and Local Group galaxies” (P.I.: F. Matteucci).

## REFERENCES

- An, D., Pinsonneault, M. H., Masseron, T., et al. 2009a, *ApJ*, 700, 523  
 An, D., Ramírez, S. V., Sellgren, K., et al. 2009b, *ApJL*, 702, L128  
 Bedin, L. R., Piotto, G., Anderson, J., et al. 2004, *ApJL*, 605, L125  
 Bennett, C. L., Larson, D., Weiland, J. L., & Hinshaw, G. 2014, *ApJ*, 794, 135  
 Bono, G., Calamida, A., Corsi, C. E., et al. 2009, in *Science with the VLT in the ELT Era*, ed. A. Moorwood (Houten: Springer), 67  
 Bono, G., Stetson, P. B., VandenBerg, D. A., et al. 2010, *ApJL*, 708, L74  
 Borysow, A. 2002, *A&A*, 390, 779  
 Borysow, A., Jorgensen, U. G., & Fu, Y. 2001, *JQSRT*, 68, 235  
 Braga, V. F., Dall’Ora, M., Bono, G., et al. 2015, *ApJ*, 799, 165  
 Bressan, A., Marigo, P., Girardi, L., et al. 2012, *MNRAS*, 427, 127  
 Buonanno, R., Buscema, G., Corsi, C. E., Ferraro, I., & Iannicola, G. 1983, *A&A*, 126, 278  
 Buonanno, R., & Iannicola, G. 1989, *PASP*, 101, 294  
 Cardelli, J. A., Clayton, G. C., & Mathis, J. S. 1989, *ApJ*, 345, 245  
 Carretta, E., Bragaglia, A., Gratton, R., D’Orazi, V., & Lucatello, S. 2009, *A&A*, 508, 695  
 Casagrande, L., & VandenBerg, D. A. 2014, *MNRAS*, 444, 392  
 Cassisi, S. 2014, *MmSAI*, 85, 498  
 Cassisi, S., Potekhin, A. Y., Pietrinferni, A., Catelan, M., & Salaris, M. 2007, *ApJ*, 661, 1094  
 Cassisi, S., Salaris, M., Pietrinferni, A., et al. 2008, *ApJL*, 672, L115  
 Cohen, J. G. 1978, *ApJ*, 223, 487  
 Cuesta, A. J., Verde, L., Riess, A., & Jimenez, R. 2015, *MNRAS*, 448, 3463  
 Davies, R., Ageorges, N., Barl, L., et al. 2010, *Proc. SPIE*, 7735, 77352A  
 De Angeli, F., Piotto, G., Cassisi, S., et al. 2005, *AJ*, 130, 116  
 Deep, A., Fiorentino, G., Tolstoy, E., et al. 2011, *A&A*, 531, A151  
 Dekel, A., Burstein, D., & White, S. D. M. 1997, in *Critical Dialogues in Cosmology*, ed. N. Turok (Singapore: World Scientific), 175  
 Dell’Omodarme, M., Valle, G., Degl’Innocenti, S., & Prada Moroni, P. G. 2012, *A&A*, 540, A26  
 Denissenkov, P. A., & Weiss, A. 2004, *ApJ*, 603, 119  
 Di Cecco, A., Faustini, F., Paresce, F., Correnti, M., & Calzoletti, L. 2015, *ApJ*, 799, 100  
 Dotter, A., Chaboyer, B., Jevremović, D., et al. 2008, *ApJS*, 178, 89  
 Dotter, A., Sarajedini, A., & Anderson, J. 2011, *ApJ*, 738, 74  
 Durrell, P. R., & Harris, W. E. 1993, *AJ*, 105, 1420  
 Dvorkin, C., Wyman, M., Rudd, D. H., & Hu, W. 2014, *PhRvD*, 90, 083503  
 Efstathiou, G. 2014, *MNRAS*, 440, 1138  
 Eisenstein, D. J., Zehavi, I., Hogg, D. W., et al. 2005, *ApJ*, 633, 560  
 Esposito, S., Riccardi, A., Pinna, E., et al. 2012, *Proc. SPIE*, 8447, 84470u  
 Esposito, S., Riccardi, A., Quirós-Pacheco, F., et al. 2010, *ApOpt*, 49, G174  
 Ferraro, F. R., Dalessandro, E., Mucciarelli, A., et al. 2009, *Natur*, 462, 483  
 Fiorentino, G., Ferraro, I., Iannicola, G., et al. 2014, arXiv:1407.2011  
 Fiorentino, G., Tolstoy, E., Diolaiti, E., et al. 2011, *A&A*, 535, A63  
 Freedman, W. L., & Madore, B. F. 2010, *ARA&A*, 48, 673  
 Freedman, W. L., Madore, B. F., Scowcroft, V., et al. 2012, *ApJ*, 758, 24  
 Gratton, R. G., Lucatello, S., Carretta, E., et al. 2012, *A&A*, 539, A19  
 Greggio, L., Falomo, R., Zaggia, S., Fantinel, D., & Uslenghi, M. 2012, *PASP*, 124, 653  
 Harris, W. E. 1996, *AJ*, 112, 1487  
 Hinshaw, G., Larson, D., Komatsu, E., et al. 2013, *ApJS*, 208, 19  
 Kraft, R. P. 1994, *PASP*, 106, 553  
 Kraft, R. P., & Ivans, I. I. 2003, *PASP*, 115, 143  
 Lagioia, E. P., Milone, A. P., Stetson, P. B., et al. 2014, *ApJ*, 782, 50  
 Leep, E. M., Wallerstein, G., & Oke, J. B. 1986, *AJ*, 91, 1117  
 Le Fèvre, O., Saisse, M., Mancini, D., et al. 2003, *Proc. SPIE*, 4841, 1670  
 Marchetti, E., Hubin, N. N., Fedrigo, E., et al. 2003, *Proc. SPIE*, 4839, 317  
 Marín-Franch, A., Aparicio, A., Piotto, G., et al. 2009, *ApJ*, 694, 1498

<sup>14</sup> [www.gmto.org/](http://www.gmto.org/)

<sup>15</sup> [www.tmt.org/](http://www.tmt.org/)

<sup>16</sup> <http://www.eso.org/sci/facilities/eelt/index.html>

- McCarthy, D. W., Jr., Ge, J., Hinz, J. L., Finn, R. A., & de Jong, R. S. 2001, *PASP*, **113**, 353
- McNamara, B. J., Harrison, T. E., & Baumgardt, H. 2004, *ApJ*, **602**, 264
- Milone, A. P., Bedin, L. R., Piotto, G., et al. 2008, *ApJ*, **673**, 241
- Milone, A. P., Marino, A. F., Bedin, L. R., et al. 2014, *MNRAS*, **439**, 1588
- Milone, A. P., Marino, A. F., Cassisi, S., et al. 2012, *ApJL*, **754**, L34
- Monelli, M., Hidalgo, S. L., Stetson, P. B., et al. 2010, *ApJ*, **720**, 1225
- Monelli, M., Milone, A. P., Stetson, P. B., et al. 2013, *MNRAS*, **431**, 2126
- Moretti, A., Piotto, G., Arcidiacono, C., et al. 2009, *A&A*, **493**, 539
- Neichel, B., Lu, J. R., Rigaut, F., et al. 2014a, *MNRAS*, **445**, 500
- Neichel, B., Rigaut, F., Vidal, F., et al. 2014b, *MNRAS*, **440**, 1002
- Osborn, W. 1971, *Obs*, **91**, 223
- Pietrinfermi, A., Cassisi, S., Salaris, M., & Castelli, F. 2004, *ApJ*, **612**, 168
- Pietrinfermi, A., Cassisi, S., Salaris, M., Percival, S., & Ferguson, J. W. 2009, *ApJ*, **697**, 275
- Pilachowski, C. A., Sneden, C., & Wallerstein, G. 1983, *ApJS*, **52**, 241
- Piotto, G., Bedin, L. R., Anderson, J., et al. 2007, *ApJL*, **661**, L53
- Piotto, G., Milone, A. P., Bedin, L. R., et al. 2015, *AJ*, **149**, 91
- Piotto, G., Villanova, S., Bedin, L. R., et al. 2005, *ApJ*, **621**, 777
- Planck Collaboration, Ade, P. A. R., Aghanim, N., et al. 2014, *A&A*, **571**, A16
- Planck Collaboration, Ade, P. A. R., Aghanim, N., et al. 2015, arXiv:1502.01589
- Pulone, L., de Marchi, G., & Paresce, F. 1999, *A&A*, **342**, 440
- Pulone, L., Salaris, M., Weiss, A., & Buonanno, R. 1998, *A&A*, **336**, L77
- Ragazzoni, R. 1996, *JMOp*, **43**, 289
- Riccardi, A., Xompero, M., Briguglio, R., et al. 2010, *Proc. SPIE*, **7736**, 2
- Riess, A. G., Filippenko, A. V., Challis, P., et al. 1998, *AJ*, **116**, 1009
- Riess, A. G., Macri, L., Casertano, S., et al. 2011, *ApJ*, **730**, 119
- Rigaut, F., Neichel, B., Boccas, M., et al. 2014, *MNRAS*, **437**, 2361
- Salaris, M., & Cassisi, S. 2015, *A&A*, **577**, A60
- Salaris, M., Degl'Innocenti, S., & Weiss, A. 1997, *ApJ*, **479**, 665
- Salaris, M., & Weiss, A. 1998, *A&A*, **335**, 943
- Salaris, M., & Weiss, A. 2002, *A&A*, **388**, 492
- Salinari, P., Del Vecchio, C., & Biliotti, V. 1994, in *European Southern Observatory Conf. and Workshop Proc. 48*, ed. F. Merkle (Garching bei München: European Southern Observatory), 247
- Sandage, A., Katem, B., & Sandage, M. 1981, *ApJS*, **46**, 41
- Saracino, S., Dalessandro, E., Ferraro, F. R., et al. 2015, *ApJ*, **806**, 152
- Sarajedini, A., Bedin, L. R., Chaboyer, B., et al. 2007, *AJ*, **133**, 1658
- Sarajedini, A., Dotter, A., & Kirkpatrick, A. 2009a, *ApJ*, **698**, 1872
- Sarajedini, A., Mancone, C. L., Lauer, T. R., et al. 2009b, *AJ*, **138**, 184
- Saumon, D., & Marley, M. S. 2008, *ApJ*, **689**, 1327
- Schlafly, E. F., & Finkbeiner, D. P. 2011, *ApJ*, **737**, 103
- Schlegel, D. J., Finkbeiner, D. P., & Davis, M. 1998, *ApJ*, **500**, 525
- Schreiber, L., Greggio, L., Falomo, R., Fantinel, D., & Uslenghi, M. 2014, *MNRAS*, **437**, 2966
- Sneden, C., Johnson, J., Kraft, R. P., et al. 2000, *ApJL*, **536**, L85
- Sneden, C., Kraft, R. P., Shetrone, M. D., et al. 1997, *AJ*, **114**, 1964
- Stetson, P. B. 1987, *PASP*, **99**, 191
- Stetson, P. B. 1994, *PASP*, **106**, 250
- Stetson, P. B., Braga, V. F., Dall'Ora, M., et al. 2014, *PASP*, **126**, 521
- Suntzeff, N. B., & Smith, V. V. 1991, *ApJ*, **381**, 160
- Suyu, S. H., Auger, M. W., Hilbert, S., et al. 2013, *ApJ*, **766**, 70
- Suyu, S. H., Marshall, P. J., Auger, M. W., et al. 2010, *ApJ*, **711**, 201
- Turri, P., McConnachie, A. W., Stetson, P. B., et al. 2014, *Proc. SPIE*, **9148**, 91483V
- Turri, P., McConnachie, A. W., Stetson, P. B., et al. 2015, *ApJ*, submitted
- VandenBerg, D. A., Bergbusch, P. A., Ferguson, J. W., & Edvardsson, B. 2014, *ApJ*, **794**, 72
- VandenBerg, D. A., Brogaard, K., Leaman, R., & Casagrande, L. 2013, *ApJ*, **775**, 134
- van den Bosch, R., de Zeeuw, T., Gebhardt, K., Noyola, E., & van de Ven, G. 2006, *ApJ*, **641**, 852
- Ventura, P., D'Antona, F., Mazzitelli, I., & Gratton, R. 2001, *ApJL*, **550**, L65
- Wyman, M., Rudd, D. H., Vanderveld, R. A., & Hu, W. 2014, *PhRvL*, **112**, 051302
- Zoccali, M., Cassisi, S., Frogel, J. A., et al. 2000, *ApJ*, **530**, 418